Chapter 8

Measuring Beam Polarization in RHIC

Our approach to measuring the beam polarization is based on the asymmetry in inclusive pion production as was chosen by the Polarization Measurement Working Group[64]. Toroid two-arm spectrometers[65] offer an attractive solution by providing left-right measurements that can cover the large energy range of RHIC and allow excellent cancellation of biases in polarization measurements. The details of this design can be found in Appendix A. Funding constraints have dictated a scaled down approach to providing a polarimeter system suitable for the initial FY2000 commissioning period. In this report, we describe a single arm pion spectrometer as well as a parallel effort to augment this with a second polarimeter based on p-Carbon scattering in the Coulomb-Nuclear Interference (CNI) region. If successful, the CNI polarimeter would be a simple, compact, and cost effective solution.

8.1 Introduction

In general, vertical beam polarization is measured by determining the asymmetry in the cross section for left and right scattering or particle production, using a reaction with a known analyzing power A_N:

$$P_B = \frac{1}{A_N(x_F, p_T)} \frac{Ed^3\sigma_L/dp^3 - Ed^3\sigma_R/dp^3}{Sum}. \tag{8.1}$$

$$P_B = \frac{1}{A_N} \frac{N_L - N_R}{N_L + N_R}. \tag{8.2}$$

P_B is the beam polarization, N_L and N_R are the number of scatters left and right normalized by luminosity. A_N can be known from experiment or theory.

For inclusive pion production, Fermilab E704 [66] has measured the analyzing power to $\Delta A_n/A_n = \pm 7\%$[1] for pion production with 200 GeV/c protons, with $x_F \sim p_\pi/p_{beam} = 0.5$ and $p_T > 0.7\ GeV/c$. For their measurement polarized protons were obtained from Λ hyperon decay and the polarization was known from the measured Λ weak decay asymmetry parameter α_Λ.

[1]The combined systematic and statistical error from E704 at 200 GeV/c is $\delta A_N/A_N = \pm 0.073$ if the statistics for both π^+ and π^- are used. If we used π^- only, the combined error is $\delta A_N/A_N = \pm 0.092$.

Recently, AGS experiment E925 measured the asymmetry at 22 GeV/c with a carbon target. Large asymmetries were observed in both π^+ and π^- production. The apparent x_F and p_t dependence of these asymmetries are consistent with the results from E704. The E925 data provide enough confidence to start construction of a relative inclusive pion polarimeter for RHIC. We may have to optimize the working kinematic region to maximize the analyzing power versus energy.

Inclusive pion production will provide an excellent polarization monitor for RHIC. A physics asymmetry is the raw (measured) asymmetry, normalized by the beam polarization. Examples are

$$A_L = \frac{1}{P_B}\frac{N_+ - N_-}{N_+ + N_-} \tag{8.3}$$

$$A_{LL} = \frac{1}{P_B^2}\frac{N_{++} - N_{+-}}{N_{++} + N_{+-}}. \tag{8.4}$$

A_L and A_{LL} are single and double spin longitudinal asymmetries. N_+ and N_{+-} are the number of scatters observed with the beam polarization helicity + (one beam + and the other beam - for N_{+-}) normalized by luminosity. The beam polarization P_B is taken as the same for both beams for A_{LL}. For those reactions with a high degree of statistical accuracy, the error in the physics asymmetry is

$$\frac{\delta A_L}{A_L} \sim \frac{\delta P_B}{P_B} \tag{8.5}$$

$$\frac{\delta A_{LL}}{A_{LL}} \sim 2\frac{\delta P_B}{P_B}. \tag{8.6}$$

Thus, if the absolute beam polarization is known to 10%, for example, then the single spin asymmetry A_L is uncertain to 10% of itself. Similarly, for A_{LL} the error becomes 20%. The beam polarization error only becomes significant when the statistical precision reaches the same level, thus at a 10σ statistical measurement for A_L and at a 5σ measurement for A_{LL}. We only anticipate a 10σ measurement for the u quark polarization in a polarized proton using parity violation of W^+ production, where the expected asymmetry A_L is quite large and, thus, the expected statistical contribution to $\delta A_L/A_L$ is small. Gluon polarization will be measured by direct photon production and the statistical contribution to $\delta A_{LL}/A_{LL}$ would approach 5σ only for maximal gluon polarization.

Our polarimeter utilizes the asymmetries (A_N, sometimes called A_p) in inclusive pion production at high x_F that were measured at the Argonne ZGS [67] at 12 GeV/c (see Fig. 8.1), at Fermilab[66] at 200 GeV/c (see Fig. 8.1), and recently at the AGS at 22 GeV/c. The asymmetries increase linearly with x_F and appear to be largely independent of the incident polarized beam momentum. Moreover, the ZGS data which were taken with both liquid hydrogen and deuterium targets, and the recent AGS data which were taken with carbon target, show little dependence on target nuclei. Since these polarimeters used a fixed target, these measurements cover most of the energy range of the RHIC beams. The pion asymmetry at the desired kinematic region measured at the AGS (E925) provides a direct measurement of the analyzing power at the RHIC injection energy.

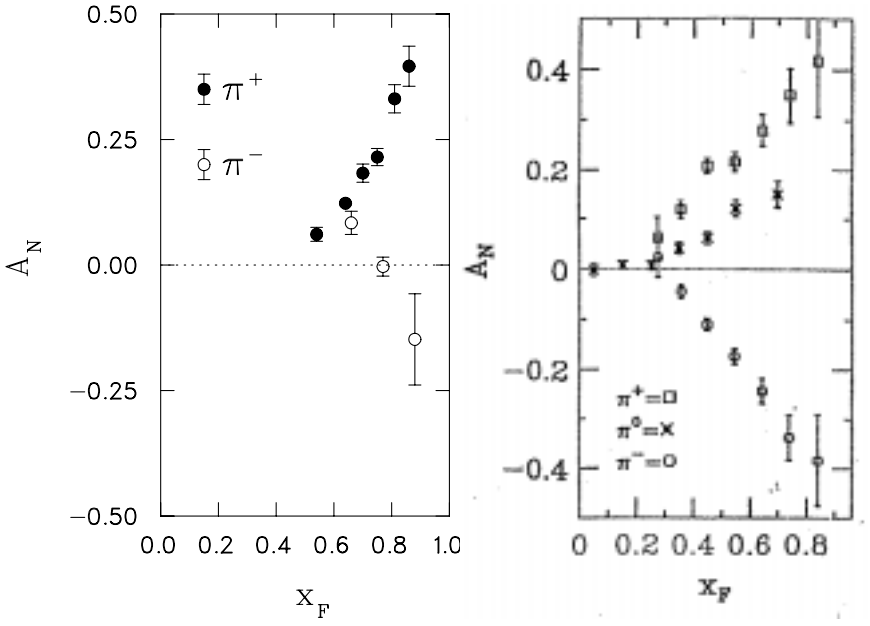

Figure 8.1: Pion asymmetries measured at ZGS (left) and in Fermilab experiment E704 (right).

The polarimeters are designed to probe the kinematic region of 0.6 in x_F and 0.8 GeV/c in transverse momentum of the pions. This was optimized from the Fermilab data based on the fact that the asymmetry in this kinematic region rises linearly with x_F while the cross section is falling as $(1 - x_F)^2$, and that the error in the asymmetry measurement is the inverse of the square root of the total number of events.

At the present stage of design, the polarimeter will allow π^- measurements. It should be noted, that since π^- are a relatively large fraction of negatives, particle identification is not necessary. Due to the large proton background, measurement of π^+ asymmetry may be difficult. At the chosen parameters, the measured π^- asymmetry is 0.14 and the invariant cross section is about 100 μb/GeV^2 [68]. The polarimeters are designed to fit in the 35 m long straight sections of the RHIC machine between Q3 and Q4. The target is located near Q4 where the vertical and horizontal lattice β functions are small thus reducing the effect of multiple scattering on emittance dilution. For this reason also, the polarimeter is placed upstream of the interaction region (see Fig. 1.2).

8.2 Measuring the Pion Asymmetry at the RHIC Injection Energy

The RHIC inclusive pion polarimeter design (see Section 8.3) will use carbon for the production target since it can survive beam heating. This presented some uncertainty as the available pion asymmetry data from the ZGS and Fermilab were collected using hydrogen and deuterium targets. The possibility that a nuclear target might present a large dilution of the observed asymmetries was a concern.

The AGS Experiment E925 was proposed to utilize an extracted polarized proton beam to provide a

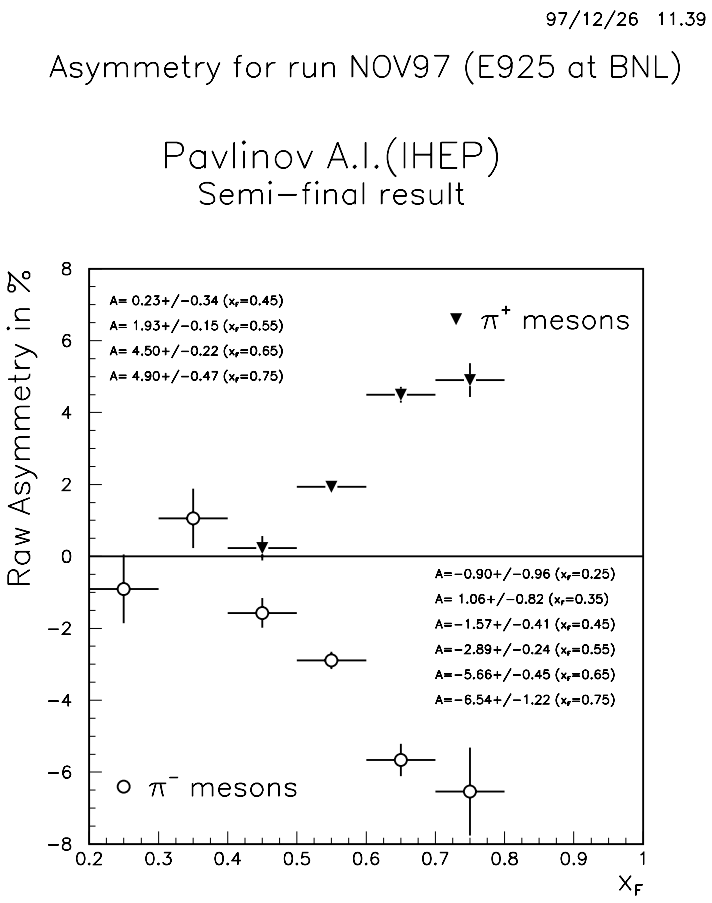

Figure 8.2: The preliminary results from AGS E925 inclusive pion production.

statistically significant measurement of the asymmetry in pion production at the RHIC injection energy around 23 GeV, to compare the data from carbon and hydrogen targets, and to assure that negative pions exhibit the same kinematic dependence at lower energies as was observed in the Fermilab data.

The E925 proposal was approved by the AGS program advisory committee in October 1996, the apparatus was installed in the AGS B1 line in February and March 1997, took low energy unpolarized beam for tune up in April and May 1997 and ran parasitically for three days at 24 GeV. The apparatus ran for one week in November 1997 with polarized beam at 21.7 GeV and a carbon target. The average beam polarization was 0.30 as measured by the local *pp* elastic scattering polarimeter.

Preliminary results are shown in Fig. 8.2. The data exhibit the mirror positive and negative pion asymmetries similar to what was seen at 200 GeV/c at Fermilab. This implies that we can use negative pions for the polarimeter as was discussed earlier. The magnitude of the asymmetry from a carbon target is (the raw asymmetries should be normalized to full beam polarization by a factor of 3.3) quite adequate for

use in the polarimeter. The dilution due to a nuclear target appears to be small. However, the comparison with production from hydrogen awaits the construction of a liquid hydrogen target which should be ready for the next polarized run scheduled for February 1999. The E925 results are quite encouraging and we are proceeding with the development of an inclusive pion polarimeter.

8.3 Scaled Down Day-one Pion Production Polarimeter

To reduce the cost, the day-one polarimeter will be a single arm spectrometer and will use modified existing apparatus. The layout is shown in Fig. 8.3. It uses five existing dipole magnets, of which the first three will be on a movable platform to allow us to reach the desired energy range 23-100 GeV/c. Four scintillator hodoscopes from the E925 will be used, two are located between dipoles 3 and 4, and the other two are after dipole 5. Due to their limited sizes, the first two hodoscopes need to move transversely for different energies to cover the energy range. The first hodoscope can be attached to the first three dipoles and the second hodoscope needs to move 8 cm to cover 23-100 GeV/c. To save power, all five dipoles will be gapped down from the original gap size of 10 cm. The last hodoscope located 24 m away from the target defines the acceptance.

Pions are produced by the interaction of polarized protons on a 5 μg/cm ^{2} carbon ribbon target about 1.5 m downstream of Q4. The string of five dipole magnets lies on the outside of the warm beam line section between Q4 and Q3. The inter-magnet drift region of 5 m is for bending particles at different energies to the same final trajectory. This arrangement provides enough space for a 6 m long Cerenkov counter and a hadron calorimeter downstream of the Cerenkov counter, should we choose to run with π^+.

The production angle and selected spectrometer momentum depend on the beam energy; at RHIC injection of 23 GeV/c, the production angle would be 58 mrad and the π momentum 13.8 GeV/c; at 100 GeV/c RHIC beam momentum, the production angle is 13 mrad and the π momentum is 60 GeV/c. The details of the layout are listed in Table 8.1. The table also includes the tunes at selected beam energies that will allow measurement in the desired kinematic range of $x_F = 0.6$ and $p_T = 0.8$ GeV/c.

8.3.1 Target Box, Beam Pipe, Pion Exit Windows

The asymmetric one-arm polarimeter gives rise to fringe fields inside the RHIC beam pipe. Only the fringe fields of the first magnet need to be considered. To save space, the first magnet has to be transversely as close to the beam pipe as possible and longitudinally as close to the target box as possible. With these constraints, there is little space for magnetic shielding. TOSCA simulations show that with a 0.05 in iron shielding and a stainless steel beam pipe (see Fig. 8.4), the vertical field in the middle of the first dipole magnet is shown in Fig. 8.5, and the fringe field in the beam pipe is shown in Fig. 8.6. It shows that the fringe field in the beam pipe center is less than 1 Gauss which is quite acceptable.

One thin carbon ribbon target will be used for both CNI and inclusive pion production. The radius of the stainless steel target box will be about 26 cm and the radius of the beam pipe in this warm straight

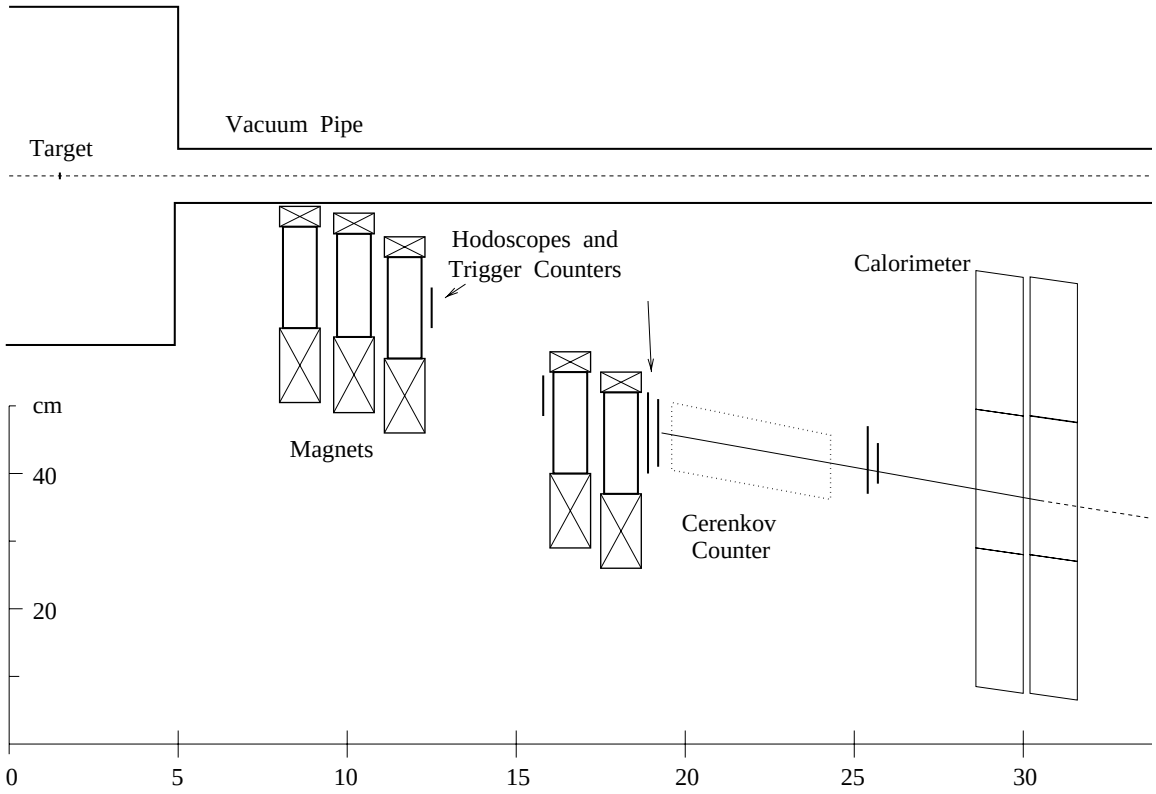

Figure 8.3: Plan view of the the one-arm polarimeter between Q4 and Q3. The first 3 dipoles are in the position for 100 GeV/c. At lower energies, the first three dipoles will move out transversely. The first two hodoscopes will also move accordingly.

	Trgt	**M1**	**M2**	**M3**	**M4**	**M5**
Longitudinal Positions (m)	1.5	8.5	9.75	11.0	16.0	17.25
Length (m)		1	1	1	1	1
Full Gap (cm)		3.7	4.3	4.9	7.8	7.8
Current (A)		920	1070	1230	1950	1950
Power (kW)		41	56	74	185	185
Transverse Positions (cm):						
23 GeV/c		31	32	35	29	33
50 GeV/c		16	17	20	29	33
75 GeV/c		11	12	15	29	33
100 GeV/c		8	9	12	29	33
Settings:						
23 GeV/c		1	1	.15	−1	−1
50 GeV/c		0.36	0	0	−1	−1
75 GeV/c		−0.15	−0.2	−1	−1	−1
100 GeV/c		−1	−1	−1	−1	−1

Table 8.1: Parameters for the polarimeter gaps and transverse positions. The transverse positions of the dipoles are with respect to the beam pipe center. The longitudinal positions of the dipoles are with respect to the end of Q4. The magnet settings are in fractions of the TOSCA design fields of 1.5T.

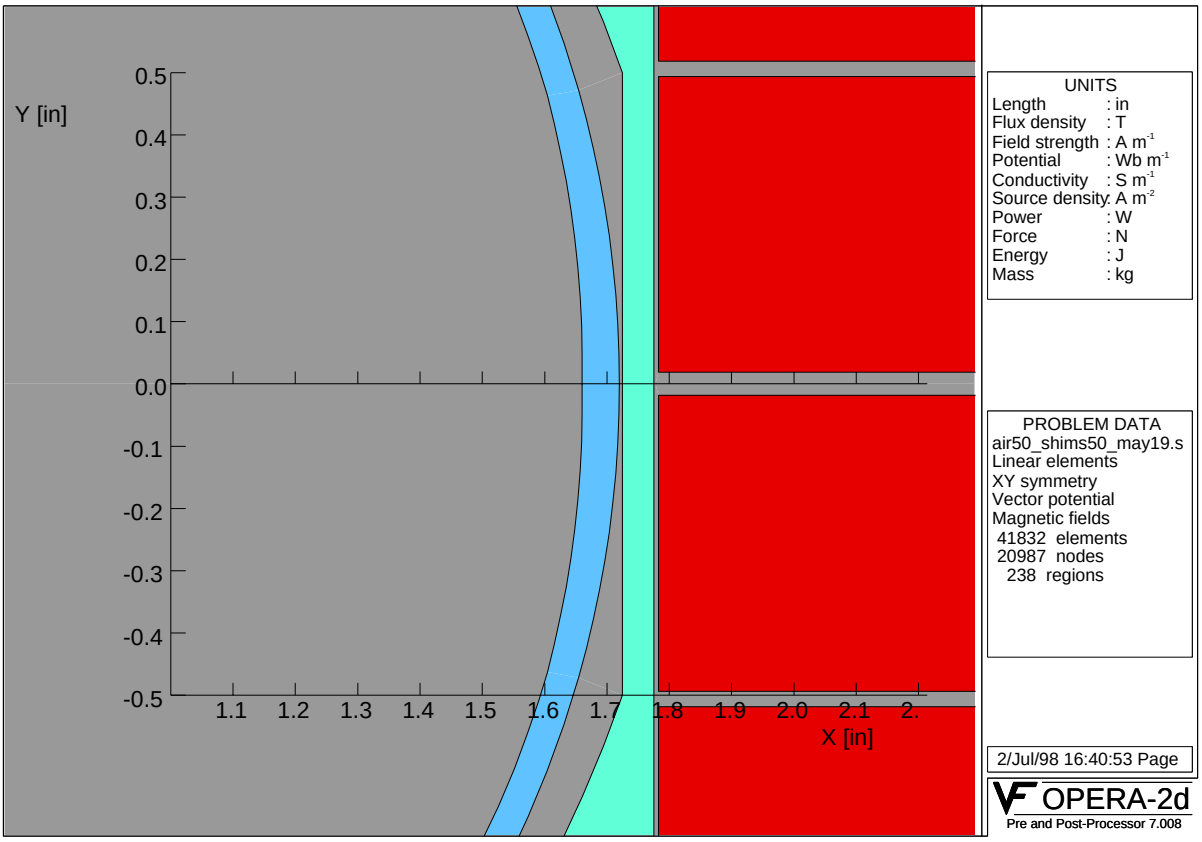

Figure 8.4: Cross-section of the first dipole magnet. The iron shield around the beam pipe is 0.05 in thick and reduces the leakage field.

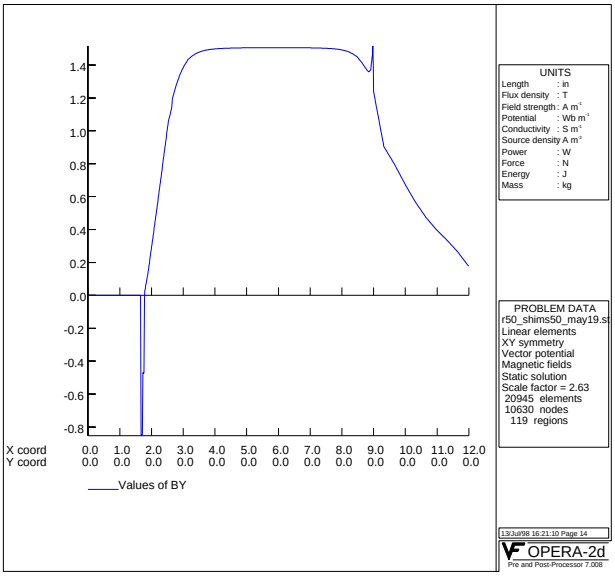

Figure 8.5: Expected vertical magnetic field strength of the dipole magnet. The vertical axis is the field strength in Tesla and the horizontal axis is the distance from the beam pipe center in inches. Note that the negative spike at about 4.4 cm is in the shielding iron.

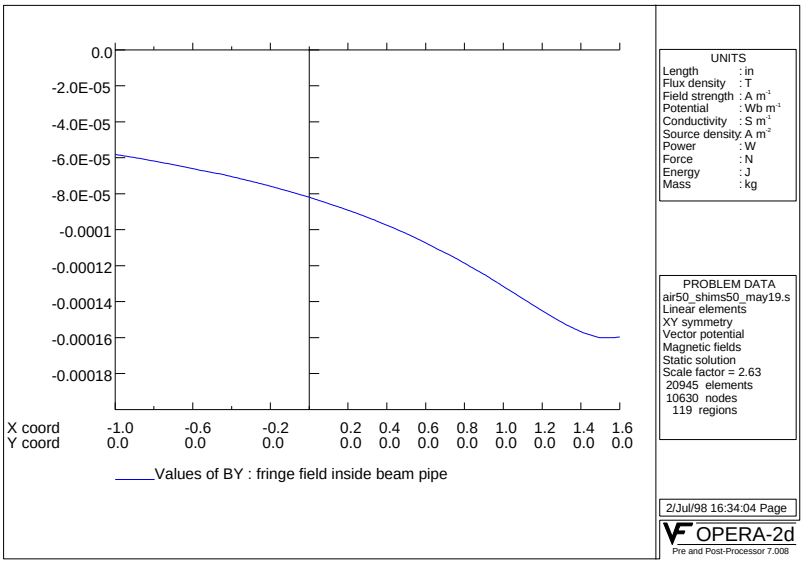

Figure 8.6: Expected fringe field of the first dipole magnet inside the beam pipe. The vertical axis is the field strength in Gauss and the horizontal axis is the distance from the beam pipe center in inches.

---

section is 4 cm. The particle exit window is 22 cm long, 3 cm wide and 0.5 mm thick. Multiple Coulomb scattering at the pion exit windows is an important issue that impacts the accuracy of track reconstruction. It is estimated that the maximum acceptable thickness of the thin window is 1mm for stainless steel. We choose a thickness of 0.5 mm[69].

8.3.2 Pion Production Target

Of the total ionization energy loss of the protons interacting with the carbon fiber, 30% is deposited on the target in the form of heat[70]. For a section of a horizontal fiber of length Δx intercepting the center of a Gaussian beam of rms width σ_x and σ_y in x and y, the heating power of the beam is,

$$P_h = \frac{\epsilon_h f_r N_p \frac{dE}{dx} \rho t_f}{2\pi\sigma_x\sigma_y} [d_f \Delta x] \tag{8.7}$$

where N_p is the number of protons in the machine, $f_r = 78$ kHz is the beam revolution frequency, $dE/dx = 1.78$ MeV/gm/cm^2 is the ionization energy loss for protons, $\rho = 1.75$ gm/cm^3 is the density , t_f is the thickness of the carbon ribbon and d_f is the diameter of the carbon fiber. The fraction of the total energy loss that is converted to heat $\epsilon_h = 0.3$, is from the CERN studies on carbon flying wires [70]. The radiated power is given by the Stefan-Boltzmann relation

$$P_{rad} = \epsilon_{rad}\sigma_{SB}(T^4 - {T_0}^4) [2 d_f \Delta x] \tag{8.8}$$

where $\epsilon_{rad} \approx 0.8$ is the emissivity, σ_{SB} is the Stefan-Boltzmann constant, T is the fiber temperature and T_0 is the ambient temperature. The expression in square brackets in Eqs. 8.7 and 8.8 is the surface area of the element. The maximum equilibrium temperature is then,

$$T_{eq} = \left(\frac{\epsilon_h f_r N_p \frac{dE}{dx} \rho t_f}{4\pi\sigma_x\sigma_y\epsilon_{rad}\sigma_{SB}} + {T_0}^4 \right)^{1/4} \tag{8.9}$$

Since the beam size depends on the energy the equilibrium temperature varies as ${p_{beam}}^{\frac{1}{4}}$. Fig. 8.7 shows the expected equilibrium temperature as a function of beam energy for a 5 μg/cm^2 carbon ribbon at full luminosity. For commissioning the heating will be less, but the target is to be used for any future polarimetry. It is generally inadvisable to run the fiber at temperatures exceeding 2000°K which is the onset of thermionic emission since this would shorten the life-time of the fiber. The result shows, with the ribbon target, heating is not a problem even with smaller beam emittance $\epsilon_N = 10\ \pi$ mm mrad. It would be advantageous to mount more than one ribbon on the driving mechanism (spaced so that the beam sees one ribbon at a time) since this would provide redundancy in case of ribbon breakage.

8.3.3 Acceptance, Event Rates and Emittance Blowup

We define ϕ as the angle between the magnet mid-plane and the pion production plane. A simple estimate of the expected θ acceptance of the system was made by numerical evaluation of the range of production

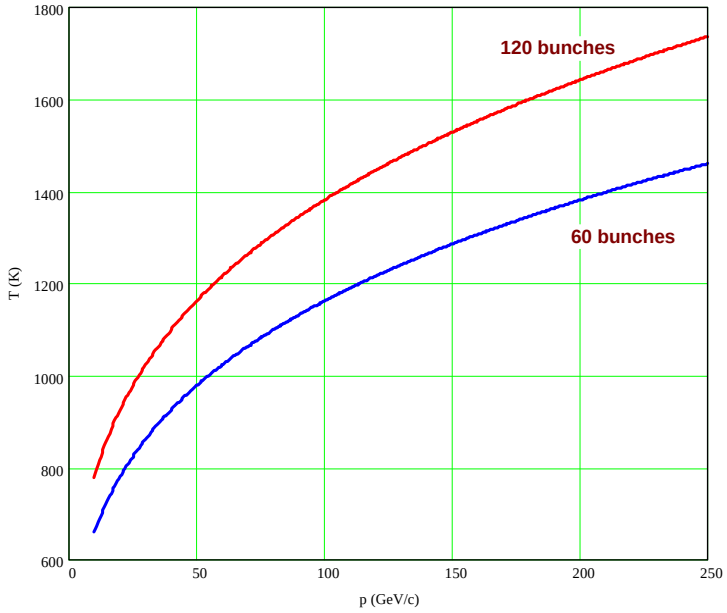

Figure 8.7: Equilibrium temperature of a 5 μg/cm^2 carbon ribbon for two beam currents. The beam parameters are: 2×10^{11} protons per bunch, 120 bunches, $\epsilon_N = 10\ \pi$ mm mrad.

angles (or p_T) that are accepted by the 11 cm hodoscope located 24 m away from the target. The plots in Fig. 8.8 show the acceptance as a function of x_F at several energy tunes. The acceptance is seen to extend to x_F and p_T values below the desired kinematic ranges of 0.6 and 0.8 GeV/c. From the ZGS, Fermilab and AGS experiments, significant asymmetries can be expected only above $x_F > 0.45$ and $p_T > 0.7$ GeV/c. It is therefore necessary that the system be able to reject low momentum pions that do not carry significant analyzing power. With the kinematic acceptance defined as $\delta x_F/x_F$ of 0.1 around x_F of 0.6, and using the p_T acceptance defined by the detectors we can estimate the event rates. The instrumental cross-section for a single polarimeter arm is

$$\delta\sigma = \left[E\frac{d^3\sigma}{dp^3}\right] p\delta p\delta\Omega \tag{8.10}$$

where $\left[E\, d^3\sigma/dp^3\right] \approx 100\ \mu\text{b/GeV}^2$ is the invariant cross-section for π^- of Ratner, et al.[68] and the solid angle $\delta\Omega$ is given by

$$\delta\Omega = \delta\theta_h\delta\theta_v \tag{8.11}$$

where $\delta\theta_h$ is the horizontal angular acceptance 0.11 m/24 m = 4.6 mrad and the vertical angular acceptance, $\delta\theta_v$ is given by

$$\delta\theta_v = 2\tan(\theta_\pi)\sin(\delta\phi) \tag{8.12}$$

with $\delta\phi$ the azimuthal acceptance half-angle of 4° and $\theta_\pi = (0.8\ \text{GeV/c})/p_L$ is the pion production angle. The number of pion events accepted in one second is given by,

$$N_{\pi,second} = f_r N_p \frac{d_w d_f}{\sqrt{2\pi}\sigma_y}\left[\frac{\rho N_A A_{nucl}}{A_w}\right]\delta\sigma \tag{8.13}$$

where d_f is the thickness of the carbon ribbon, d_w is the width of the carbon ribbon, $A_{nucl} = 12$ is the number of nucleons/atom, $A_w = 12$ gm/mole is the atomic weight of carbon and $N_A = 6.022 \times 10^{23}$ atoms/mole.

As the target sits in the beam the emittance of the beam is increased due to multiple scattering. The resulting addition to the normalized 95% emittance in one second can be estimated from

$$\Delta\epsilon_{(x,y)second} = \frac{d_f d_w f_r}{\sqrt{2\pi}\sigma_y}\frac{3\beta_{(x,y)}}{\beta^3\gamma}\frac{1}{L_{rad}}\left(\frac{0.0141}{0.938}\right)^2[\pi] \tag{8.14}$$

where $\beta_{(x,y)}$ is the (x, y) lattice beta function at the target location, β and γ are the usual relativistic factors and $L_{rad} = 18.8$ cm is the radiation length of the target material. It is useful to parameterize the resulting total emittance growth in terms of the total pion statistics N_π,

$$\Delta\epsilon_{(x,y)tot} = \frac{3\beta_{(x,y)}}{\beta^3\gamma}\frac{1}{L_{rad}}\left[\frac{0.0141}{0.938}\right]^2\frac{N_\pi}{N_p}\left[\frac{A_w}{\rho N_A A_{nucl}}\right]\frac{1}{\delta\sigma}[\pi]\,. \tag{8.15}$$

With the relations given above we estimate the event rates and measuring times. These are listed in Table 8.2. We used a 5 μg/cm^2 carbon ribbon target, a pion momentum bite of 0.1, at $x_F = 0.6$, and $p_T = 0.8$ GeV/c. We have assumed a total statistics of 10^4 pions in the polarimeter to obtain a 7% error

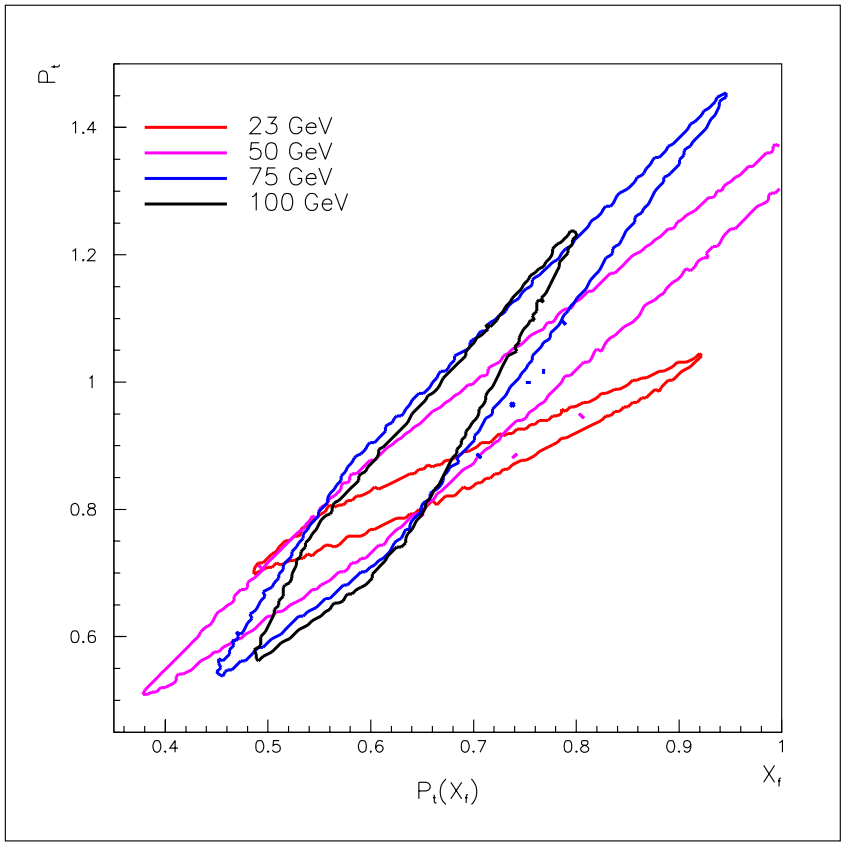

Figure 8.8: Polarimeter acceptance for 23 GeV/c, 50 GeV/c, 75 GeV/c and 100 GeV/c using respective magnet settings found in Table 8.1.

p_π (GeV/c)	$\delta\Omega$ (μster)	$\delta\sigma$ (nb)	T_{meas} (sec)	$\Delta\epsilon_x$ ($\Delta\epsilon_y$) (π mm mrad)
60	6.4	231	1.9	0.0028 (0.0032)
13.8	26.1	49.7	~ 18	0.22 (0.33)

Table 8.2: Acceptance and rate estimates for the pion polarimeter. Also includes expected emittance dilution due to multiple scattering for collecting 10^4 pions. The following parameters were assumed: $\epsilon_N = 20\pi$ mm mrad, protons/fill = 120 bunches at 2×10^{11} protons/bunch, $d_f = 2.5 \times 10^{-8}$ m, $p_T = 0.8$ GeV/c, $\delta p/p = 0.1$

1st hodoscopes	3-4 × 5 cm	X
2nd hodoscopes	3-4 × 7 cm	X
3rd hodoscopes	8-10 × 4 cm	X,Y
4th hodoscopes	10 × 10 cm	X,Y

Table 8.3: Sizes of the four hodoscopes.

in polarization. The emittance growth at 23 GeV/c is about 1% for the measurement, and there is much less growth for higher energy. Thus, the measurements can be parasitic. As can be seen from the table, measurement times are quite reasonable. The acceptance, and number of bunches used (for example, for commissioning) will be optimized, since these choices depend on the number of stored protons, rates in the detector, and the desired polarization error. In year-one commissioning, the number of bunches will be about 60, and the intensity of each bunch is estimated as half of the designed value: 1×10^{11} protons/bunch. The measuring time and emittance blow up are estimated as 72 s and 0.8π mm-mrad, respectively for the injection energy.

8.3.4 Polarimeter Detectors

The detectors will determine the (x_F, p_T) for each particle, and crudely measure the energy of each particle. If π^+ measurement becomes necessary in the low intensity situation, a Cerenkov counter will be used to identify pions. The (x_F, p_T) measurement will allow selection of pions with high analyzing power. We will want to choose pions with $x_F > 0.47$ and $p_T > 0.6$ GeV/c. The acceptance of the dipoles extends to lower (x_F, p_T) where pion production is significantly larger (see Fig. 8.8) and the analyzing power lower. Therefore, the lower edge of (x_F, p_T) for the selected pions must be sharply defined. Four scintillator hodoscopes modified from AGS E925 will be used (see Table 8.3). Each element is 6 mm wide scintillator and two staggered, overlapping layers of the scintillator provides 2 mm wide segments. There are two hodoscopes between the third and fourth dipoles, and the other two hodoscopes are after the fifth dipole. In addition, there are three trigger scintillators near hodoscopes 2-4. Since a large analyzing power for π^- production at the RHIC injection energy has been found in AGS E925, we expect to use only π^-. We plan to use tracking to measure (x_F, p_T) and, in addition, hadron calorimeters to provide a cruder but independent measurement of the pion energy. The calorimeters will be built with existing modules.

An important detector issue is to isolate the detectors out of the line of sight of the target. For year-one operation, the intensity is low and simulation shows that the direct particles are not a problem. To reconstruct the pion trajectories we use the target/beam location as an upstream point, and we measure the deflection (r) and track angle (Θ_{meas}) after the bending in the dipoles (see Fig. 8.3).

Resolution, with $\delta x = 1$ mm from the hodoscopes, is $\delta p/p = 1.1\%$ with no multiple scattering (1.5% with scattering), and $\delta\Theta/\Theta = 0.5\%$. This is good enough to be used to select higher x_F and p_T for good analyzing power, and to match the acceptance of E925 to use A_N measured there. The separation of Θ (basically given by the position at hodoscope 1) and momentum (basically the difference between positions

at hodoscope 3 and hodoscope 4) is also nice in that matrix logic can be used as a clean trigger to eliminate the low analyzing power region.

It is important to have a deadtimeless data acquisition. Otherwise, we blow up the beam with the target, and do not get as much data as we need. We can take advantage of the small amount of data per measurement and place all the data into memory, reading it out after 10^4 pions have been recorded. A LeCroy 2367 with 3 MByte memory, and internal logic to trigger with a lower x_F and p_T cut would allow 0.5 million events to be stored by using two units (there are 57 input/output lines available per unit).

8.4 p-Carbon CNI Polarimeter

Small angle elastic scattering of hadrons in the Coulomb-Nuclear Interaction (CNI) region has long been advocated for polarimetry. The predicted asymmetry is significant and largely independent of energy for energies above a few GeV. The prediction rests on hadronic spin flip being small, which is expected for high energies. The CNI process has been proposed for RHIC polarimetry using a hydrogen jet target and in collider mode using the *pp*2*pp* experiment. Both would be *pp* CNI. It is also possible to use a carbon target, *pC* CNI, which is simpler and cheaper than a hydrogen jet, and can be installed in the individual rings, as opposed to requiring collision of both rings as for the *pp*2*pp* experiment. The analyzing power for *pC* CNI is similar to *pp* CNI (both about 0.04) and the cross section is high, giving a very large figure of merit NA^2. However, for *pC* CNI, the proton scattered forward is not easily detectable (it stays within the beam), and the energy of the recoil carbon nucleus is 100-400 keV. The low energy carbon would stop in most targets. The *pC* CNI polarimeter became feasible with the development of very thin ribbon carbon targets at IUCF[71]. The slowness of the recoil carbon also makes detection difficult. However, the arrival time of the carbon can be set to be in between RHIC bunches, avoiding prompt background.

Elastic scattering in the small angle CNI region is predicted to have a calculable analyzing power of about 3-5%[72] as well as a large cross section over the whole RHIC energy range from 23 GeV/c to 250 GeV/c. The analyzing power is given by

$$A_N = \frac{G t_0 t \sqrt{t}}{m_p (t^2 + t_0^2)}, \tag{8.16}$$

where G is the anomalous magnetic moment of the proton(1.7928), m_p the proton mass, and $t_0 = \frac{8\pi\alpha Z}{\sigma_{tot}}$. The total cross section σ_{tot} is only weakly energy dependent over the relevant energy range. Fig. 8.9 shows the calculated analyzing power for a hydrogen target ($Z = 1$, $\sigma_{tot} = 35$ mb) and a carbon target($Z = 6$, $\sigma_{tot} = 330$ mb[73]) as a function of $(-t)$. The uncertainty from a hadronic spin flip amplitude has been estimated to be smaller than 10% of the analyzing power from CNI. Using a carbon target will result in the high luminosity required for fast polarization measurements. The sizable analyzing power, the large cross section and the advantages of a solid ribbon target makes this process ideal for a fast primary polarimeter for RHIC.

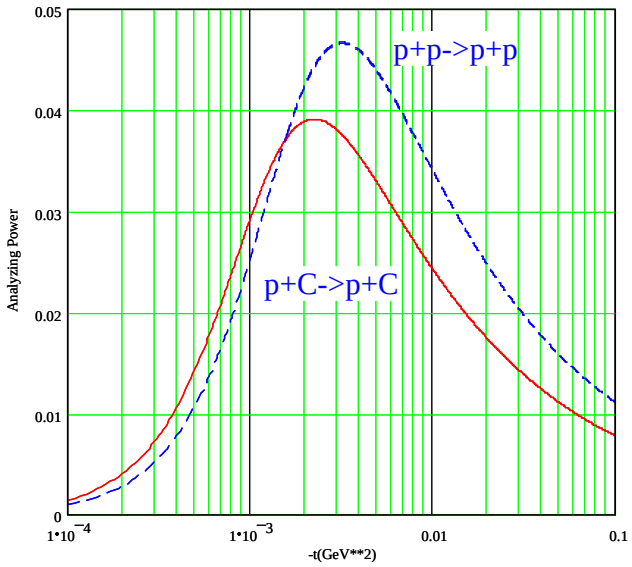

Figure 8.9: Coulomb-Nuclear interference analyzing power for pp and pC scattering.

A typical $(-t)$ value of 0.002 to 0.01 GeV^2 results at high energy in a very small angle of the forward scattered proton relative to the beam direction and also a very low kinetic energy of the Carbon recoil of about 0.5 MeV. It will be impossible to measure the forward scattered proton without drastically reducing the beam divergence at the target which would severely reduce the scattering rate and also cause unacceptable beam emittance growth. It will therefore be necessary to rely only on the measurement of the recoil Carbon nucleus to identify elastic scattering.

Direct measurement of the 0.1 to 1 MeV recoil Carbon nucleus is only possible for a very thin Carbon target. The detector for the recoil carbon must be compact with recoil arms about 10 cm long, and in the beam vacuum. The detector will be silicon strip detector (SSD) and/or micro-channel plate (MCP) with sizes of the order of centimeters. Very thin micro-ribbon carbon targets are needed to allow the recoils to exit.

The determination of elastic scattering will be done by measuring both the energy and angle of the recoil Carbon. In addition, the time-of-flight will be measured to discriminate against target fragments. Fig. 8.10 shows the expected energy-angle correlation for the recoil Carbon. The horizontal lines show the expected angular straggling from the target ribbon. Also shown is the kinematic range for producing the first excited Carbon state at 4.4 MeV. Elastics are well separated. Another background would be forward production of N^* which needs to be evaluated. The kinematics of the recoil system will not separate this background.

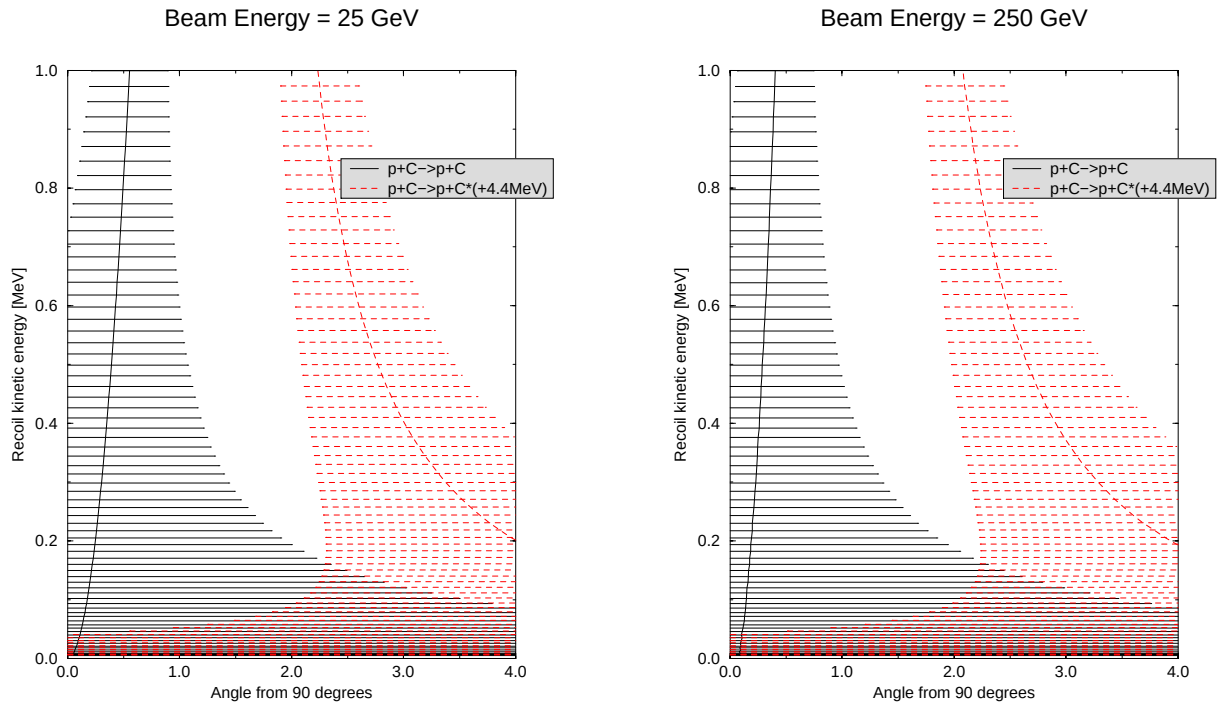

Figure 8.10: Energy-angle correlation for the elastic and inelastic recoil Carbon nucleus at 25 GeV (left) and 250 GeV (right).

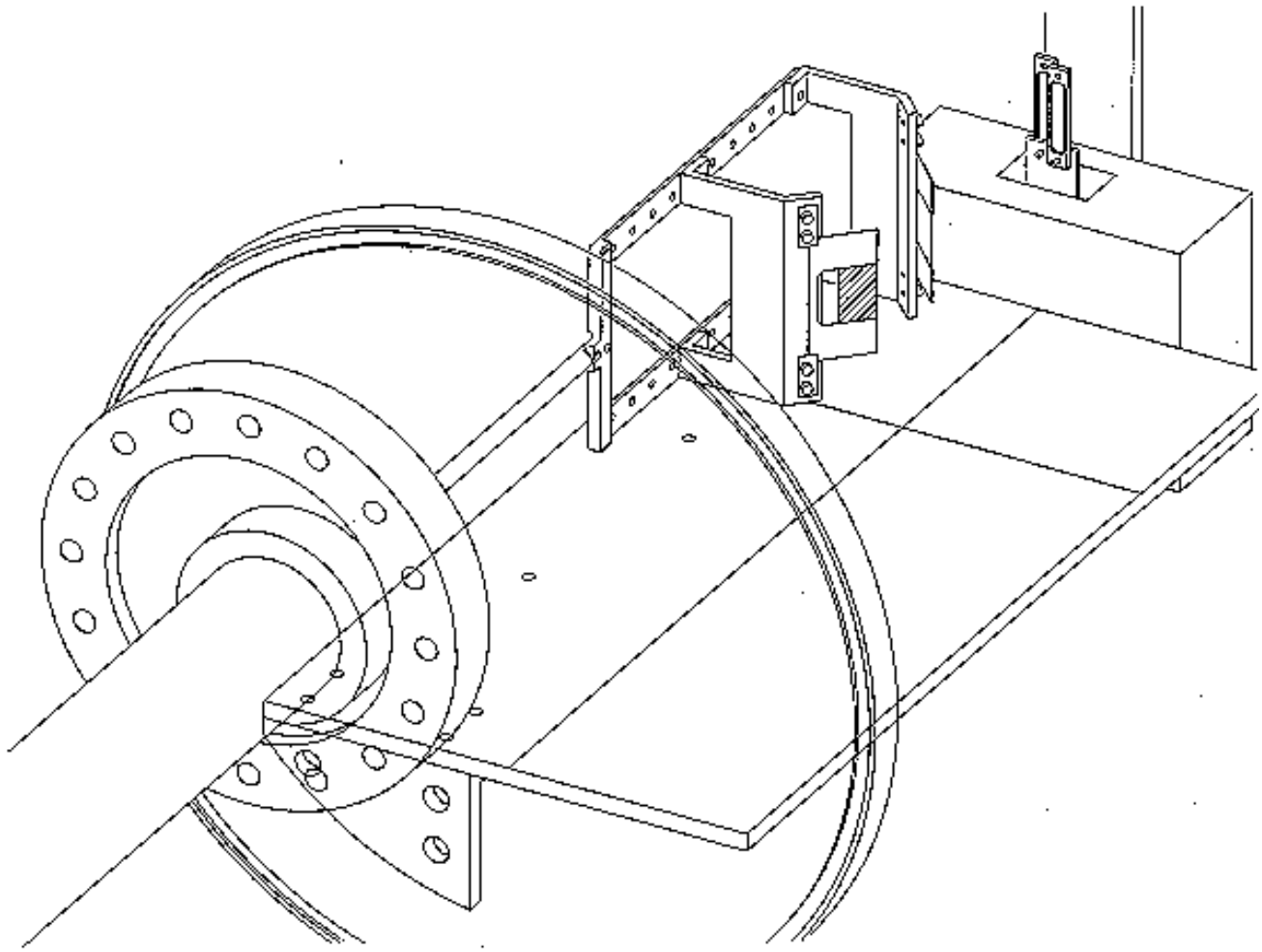

Figure 8.11: The layout of the IUCF 200 MeV small angle elastic p-carbon scattering experiment. The two silicon detectors are mounted on the far side, and the foil (near) and ribbon (far) targets are mounted on the movable fork. The beam passes between the two targets, from right to left in this figure.

A proposal[74] was presented and approved by IUCF to carry out tests of such a polarimeter using silicon detectors which had its first successful run in March 1998. The layout of this test is shown in Fig. 8.11. For low energy and kinematics where the recoil carbon is 0.1 to 1 MeV, the forward proton scatters to a large angle, and can be seen by the Meyer forward detector system at IUCF[75]. Fig. 8.12 shows the results from the March test. The energy in the silicon is shown in (a), the correlation between the forward proton scattering angle and carbon energy in (b), the correlation between time of flight at the silicon (the start time used for this was the rf time) is shown in (c), and the projection of the proton plane onto a plane transverse to the beam is shown in (d) after an energy cut on the silicon has been applied. The carbon energy range for this silicon detector was 150-400 keV. For the data in (a), (b) and (d), the proton detector was used to trigger (half the detector, as can be seen from (d)). We also successfully triggered

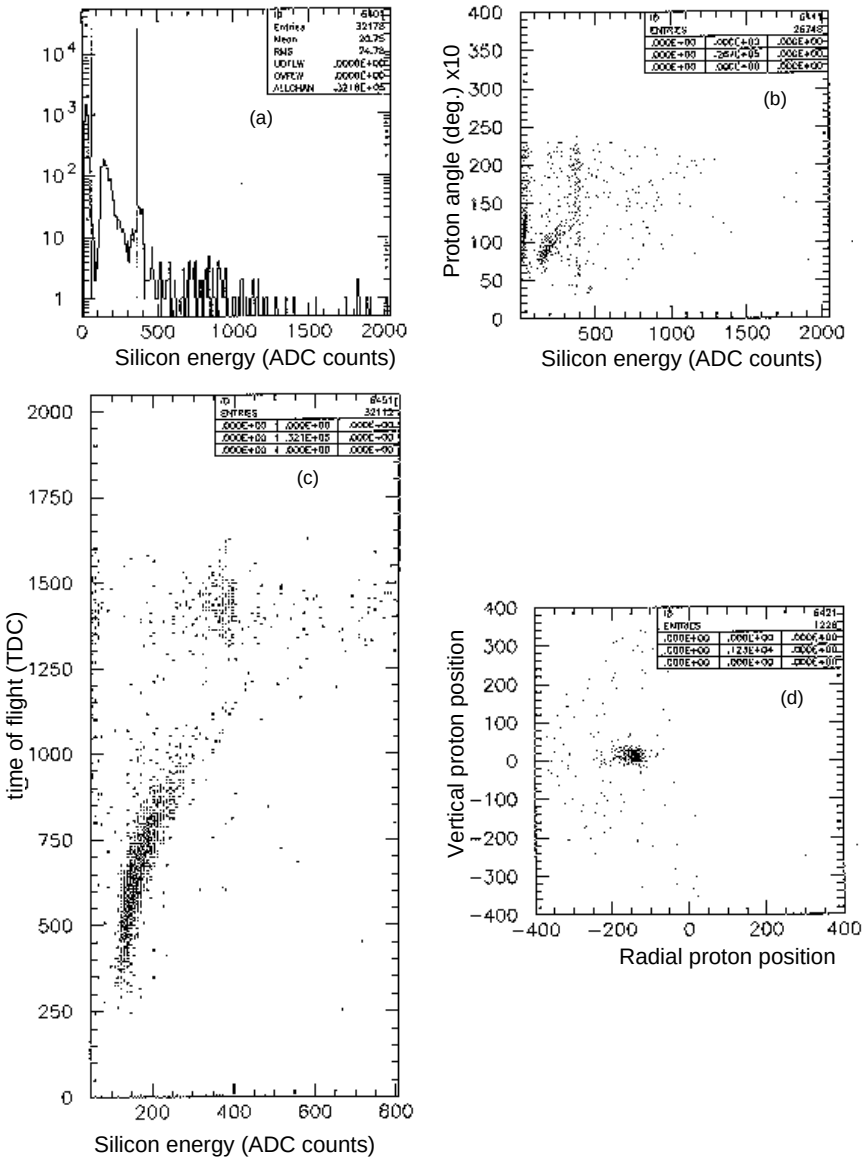

Figure 8.12: Results from IUCF pC test run. (a) Top left, energy in silicon detectors. (b) Top right, forward proton energy and carbon energy correlation. (c) Bottom left, time of flight correlation. (d) Bottom right, space projection of elastically scattered protons.

on only the silicon detector energy (e), with the difficulty that a higher threshold was necessary (300 keV) due to noise background. This is one of the issues we are continuing to study.

Simultaneously, our collaborators at Kyoto University and RIKEN are conducting similar tests using Micro Channel Plate (MCP) detectors at the Kyoto 10 MeV proton Van de Graaff.[76] The first test used a micro channel plate to directly observe the recoil carbon. Time of flight is used to give the carbon energies, shown in Fig. 8.13. The forward proton is observed and the predicted energy for each histogram is indicated. The second test used an electrostatic mirror, as shown in Fig. 8.14. Electrons emitted from the surface of the silicon were collected in the MCP. The silicon was not read out. Results are shown in Fig. 8.15. For carbon below 400 keV, the efficiency for electron emission from silicon was poor. A new test this fall will use a thin carbon foil to emit secondary electrons, with the goal of reaching lower energy (100-200 keV). The setup is shown in Fig. 8.16. This would be our ideal detector: a coincidence between the MCP (time and angle) and silicon (energy and angle).

Our next plan is to install such a polarimeter in the AGS for the upcoming run in February 1999. This will be used to measure A_N for the RHIC injection energy and to test the technique at higher energy. If this is a success, we plan to install a two-arm pC CNI detector for the commissioning of RHIC in FY2000. The pC CNI and pion polarimeters would use the same carbon ribbon target.

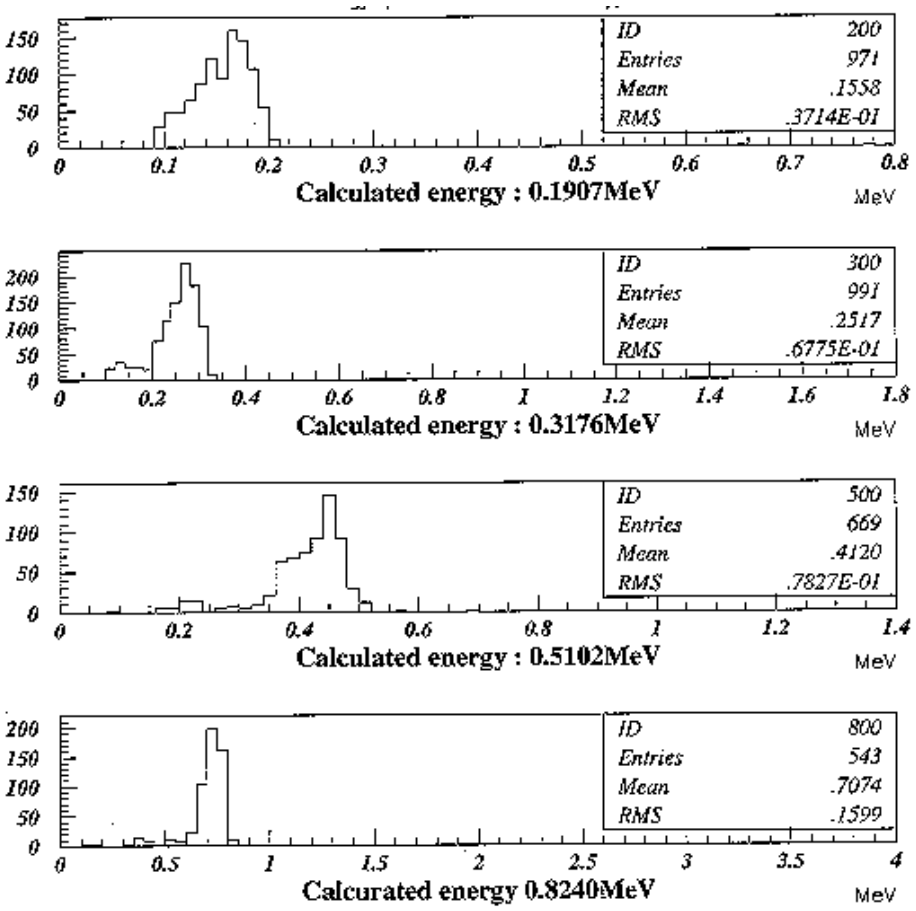

Figure 8.13: The experiment data from Kyoto University Van de Graaff with only MCP used.

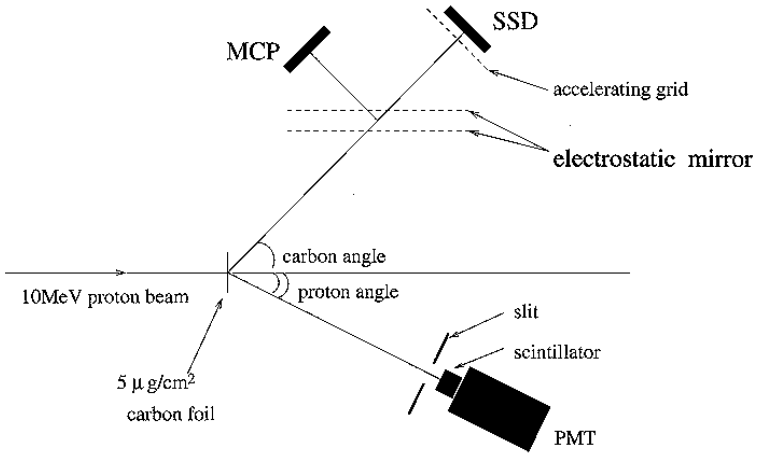

Figure 8.14: The experiment layout at Kyoto University Van de Graaff.

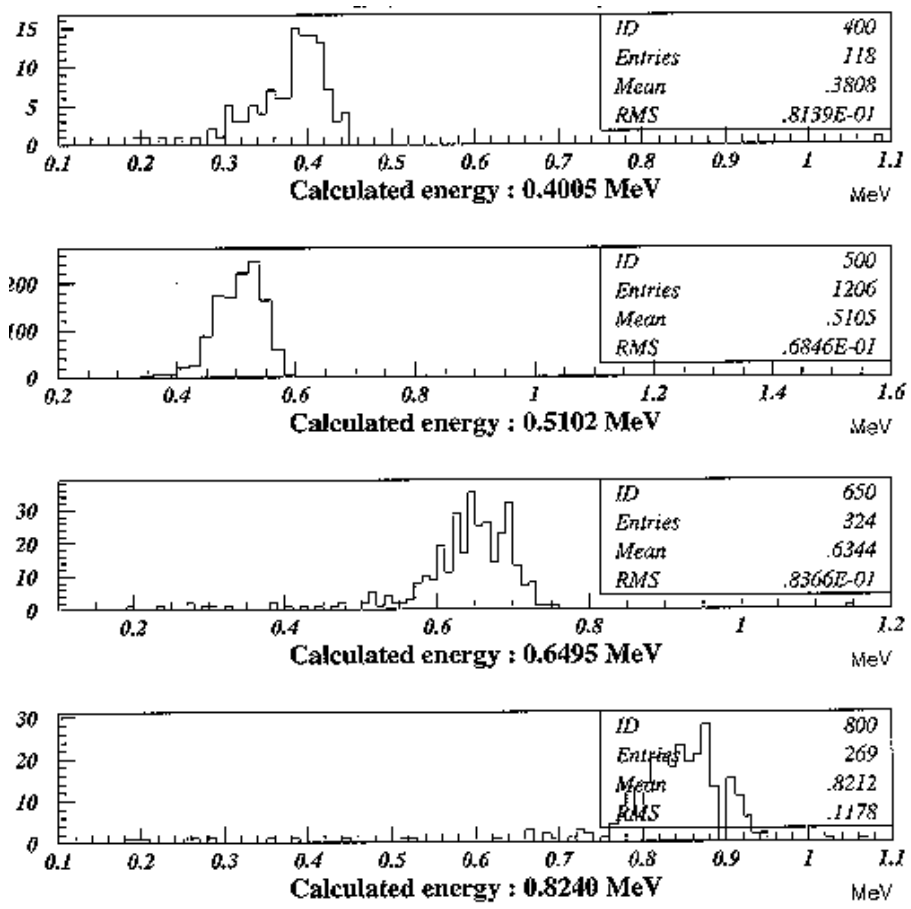

Figure 8.15: The experiment data from Kyoto University Van de Graaff with both MCP and SSD used (see Fig. 8.14).

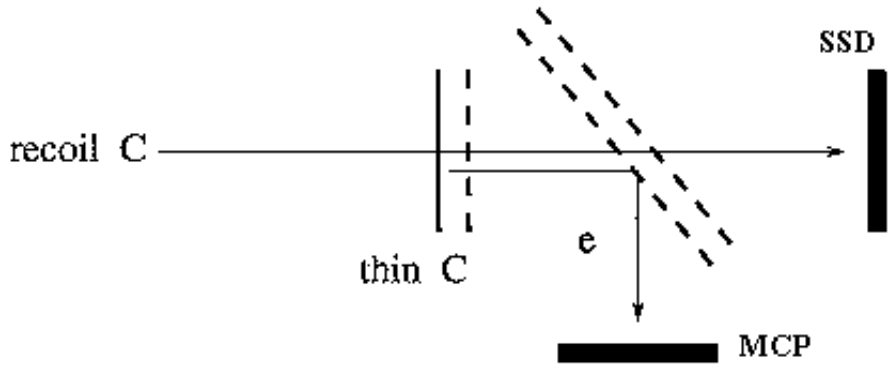

Figure 8.16: The detector system to be tested in the future.